ADVANCES IN ATMOSPHERIC SCIENCES, VOL. 37, MAY 2020, 431–440

• **Original Paper** •

Antarctic Radiosonde Observations Reduce Uncertainties and Errors in Reanalyses and Forecasts over the Southern Ocean: An Extreme Cyclone Case

Kazutoshi SATO*[1,2], Jun INOUE[3,4,2], Akira YAMAZAKI[2], Naohiko HIRASAWA[3,4], Konosuke SUGIURA[5], and Kyohei YAMADA[3]

[1]*Kitami Institute of Technology*, *Kitami* 090-8507, *Japan*

[2]*Application Laboratory*, *Japan Agency for Marine-Earth Science and Technology*, *Yokohama* 236-0001, *Japan*

[3]*National Institute of Polar Research*, *Tachikawa* 190-8518, *Japan*

[4]*SOKENDAI (Graduate University for Advanced Studies)*, *Hayama* 240-0193, *Japan*

[5]*University of Toyama*, *Toyama* 930-8555, *Japan*

(Received 22 October 2018; revised 21 April 2019; accepted 30 April 2019)

ABSTRACT

Cyclones with strong winds can make the Southern Ocean and the Antarctic a dangerous environment. Accurate weather forecasts are essential for safe shipping in the Southern Ocean and observational and logistical operations at Antarctic research stations. This study investigated the impact of additional radiosonde observations from Research Vessel "Shirase" over the Southern Ocean and Dome Fuji Station in Antarctica on reanalysis data and forecast experiments using an ensemble data assimilation system comprising the Atmospheric General Circulation Model for the Earth Simulator and the Local Ensemble Transform Kalman Filter Experimental Ensemble Reanalysis, version 2. A 63-member ensemble forecast experiment was conducted focusing on an unusually strong Antarctic cyclonic event. Reanalysis data with (observing system experiment) and without (control) additional radiosonde data were used as initial values. The observing system experiment correctly captured the central pressure of the cyclone, which led to the reliable prediction of the strong winds and moisture transport near the coast. Conversely, the control experiment predicted lower wind speeds because it failed to forecast the central pressure of the cyclone adequately. Differences were found in cyclone predictions of operational forecast systems with and without assimilation of radiosonde observations from Dome Fuji Station.

Key words: radiosonde, data assimilation, TIGGE, Antarctica, weather forecast

Citation: Sato, K., J. Inoue, A. Yamazaki, N. Hirasawa, K. Sugiura, and K. Yamada, 2020: Antarctic radiosonde observations reduce uncertainties and errors in reanalyses and forecasts over the southern ocean: an extreme cyclone case. *Adv. Atmos. Sci.*, **37**(5), 431−440, https://doi.org/10.1007/s00376-019-8231-x.

Article Highlights:

- Assimilation of additional Antarctic radiosonde observations improved skill in forecasting the strong winds associated with an Antarctic cyclone.
- Uncertainty originating from excluding additional Antarctic observations extended across the Southern Ocean, even in reanalysis data.
- Assimilation of additional radiosonde observations improves cyclone forecasts in operational forecast systems.

1. Introduction

Reanalysis data are derived from past observation data and atmospheric parameters obtained from a weather forecasting model (e.g., Saha et al., 2010, 2014; Dee et al., 2011; Kobayashi et al., 2015; Gelaro et al., 2017). Reanalysis datasets are important for the study of the atmospheric circulation over the Southern Ocean, and previous studies have reported the superior performance of ERA-Interim reanalysis dataset in reproducing the atmospheric circulation over the polar regions (Inoue et al., 2011; Jones et al., 2015). The ERA-Interim dataset has been used for assessing surface mass balance (Gorodetskaya et al., 2014) and as initial conditions for regional models (Rinke et al., 2012, 2013). However, there can be biases in the main parameters of

* Corresponding author: Kazutoshi SATO
Email: satokazu@mail.kitami-it.ac.jp

interest of the polar regions, such as temperature, specific humidity, and wind speed, in reanalysis data; biases can be particularly prevalent in the lower troposphere (Inoue et al., 2011; Jakobson et al., 2012; Bracegirdle and Marshall, 2012; Bracegirdle, 2013; Jones and Lister, 2015; Jones et al., 2016). As a result, reproduction of atmospheric circulation depends on model performance as well as the sparse observational data from the polar regions (e.g., temperature and specific humidity) that can be assimilated. In recent decades, biases in reanalyses have been reduced by making use of extensive satellite data (Dee et al., 2011; Bromwich et al., 2011; Jung and Matsueda, 2016); however, biases remain both at the surface and at upper levels in polar regions (Jung et al., 2016).

Similar biases are also seen in analysis data, which combine short-range forecasts with observational data (Powers et al., 2007, Yamagami et al., 2017). This can cause differences in the reproduction of atmospheric circulation and lead to substantial errors in weather forecasts because analysis data are used to initialize operational weather forecasts (Yamagami et al., 2017). The magnitude of such errors can be reduced not only by improvement of model performance but also by an increase in the quantity of observational data that is combined with the forecast data. Using observing system experiments (OSEs), previous studies have demonstrated that incorporation of additional Arctic radiosonde observations can influence the reproduction of atmospheric circulation of upper-level troughs in analyses and weather forecasts over the Northern Hemisphere (Inoue et al., 2009, 2013, 2015; Kristjánsson et al., 2011; Yamazaki et al., 2015; Sato et al., 2017, 2018a). Incorporation of Arctic drifting buoy data reduces the uncertainty (ensemble spread) of simulated sea level pressure (SLP) over sea ice; however, the effect has been limited to the lower troposphere (Inoue et al., 2009). Additional Arctic radiosonde observations, which reduce the ensemble spread at the upper levels in analysis data, have improved the accuracy of forecasts of surface circulation over the Arctic Ocean (Kristjánsson et al., 2011; Yamazaki et al., 2015; Inoue et al., 2015) and of midlatitude cyclones (Sato et al., 2017; 2018a). In contrast, few studies have conducted OSEs using Antarctic observations, where the impact of additional radiosonde observations would be expected to extend over a wide area because of the lack of data near the South Pole (Semmler et al., 2016). Inclusion of radiosonde data reduces the ensemble spread at upper levels over the Southern Hemisphere and improves the forecast skill over the midlatitudes in the Southern Hemisphere (Sato et al., 2018b; Soldatenko et al., 2018). However, no previous study has reported impacts of the incorporation of additional radiosonde data collected from Antarctic coastal regions and research stations on weather forecasts of the Southern Hemisphere.

During the 59th Japanese Antarctic Research Expedition, various atmospheric and oceanographic observations were performed over the Southern Ocean and Antarctica, including surface meteorological observations at the Japanese Syowa Station. On 3 January 2018, a cyclone developed over the Southern Ocean (Fig. 1a), which caused winds exceeding 30 m s^{-1} at Syowa Station. During December 2017, radiosonde observations were conducted near Syowa Station by Research Vessel (RV) "Shirase" (Fig. 1b). Furthermore, additional radiosonde observations were also undertaken at Dome Fuji Station between December 2017 and January 2018. This study investigated the impact of these additional radiosonde observations on the reproduction of the cyclone using an ensemble data assimilation system and a forecast experiment.

2. Data

2.1. *Additional radiosonde observations from RV Shirase and Dome Fuji Station*

RV Shirase sailed to Syowa Station (69.00°S, 39.58°E) in December 2017. She departed Fremantle (Australia) on 2 December 2017 and crossed the Southern Ocean, arriving at Syowa Station on 17 December. She was moored at Syowa Station between 18 December 2017 and 3 March 2018. Radiosondes were launched from the ship at 1200 and 1800 UTC between 14 and 19 December (Fig. 1b). In addition, radiosondes were launched from Dome Fuji Station (77.8°S, 39.1°E; after 30 December: 77.6°S, 41.0°E) at 1200 and 1800 UTC between 19 December 2017 and 2 January 2018. Meisei RS-06G radiosondes, developed by the Japanese company Meisei Electric Co. Ltd., were used for these additional observations.

2.2. *Ensemble data assimilation system*

The Atmospheric General Circulation Model for the Earth Simulator (AFES; Ohfuchi et al., 2004; Enomoto et al., 2008) and the Local Ensemble Transform Kalman Filter (LETKF; Hunt et al., 2007; Miyoshi and Yamane, 2007) Experimental Ensemble Reanalysis, version 2 (ALERA2), comprise an ensemble data assimilation system—the so-called AFES–LETKF Ensemble Data Assimilation System, version 2 (ALEDAS2; Enomoto et al., 2013). ALEDAS2 is composed of AFES with a horizontal resolution of T119 (triangular truncation with truncation wavenumber 119, 1° × 1°) and 48 vertical levels and an LETKF. The ALERA2 datasets reproduce the geopotential height and temperature structures of large-scale circulation in the troposphere and lower stratosphere, as well as other reanalysis products (Inoue et al., 2013; Yamazaki et al., 2015; Sato et al., 2017, 2018a). AFES provides 63-member ensemble forecasts. The assimilated observations were adapted from the PREPBUFR Global Observation datasets of the National Centers for Environmental Prediction (NCEP) that are archived at the University Corporation for Atmospheric Research. Although wind data obtained by satellite and aircraft were assimilated into ALERA2, satellite radiance data were removed. The National Oceanic and Atmospheric Administration daily Optimum Interpolation Sea Surface Temperature, version 2, was used for ocean and sea-ice boundary conditions

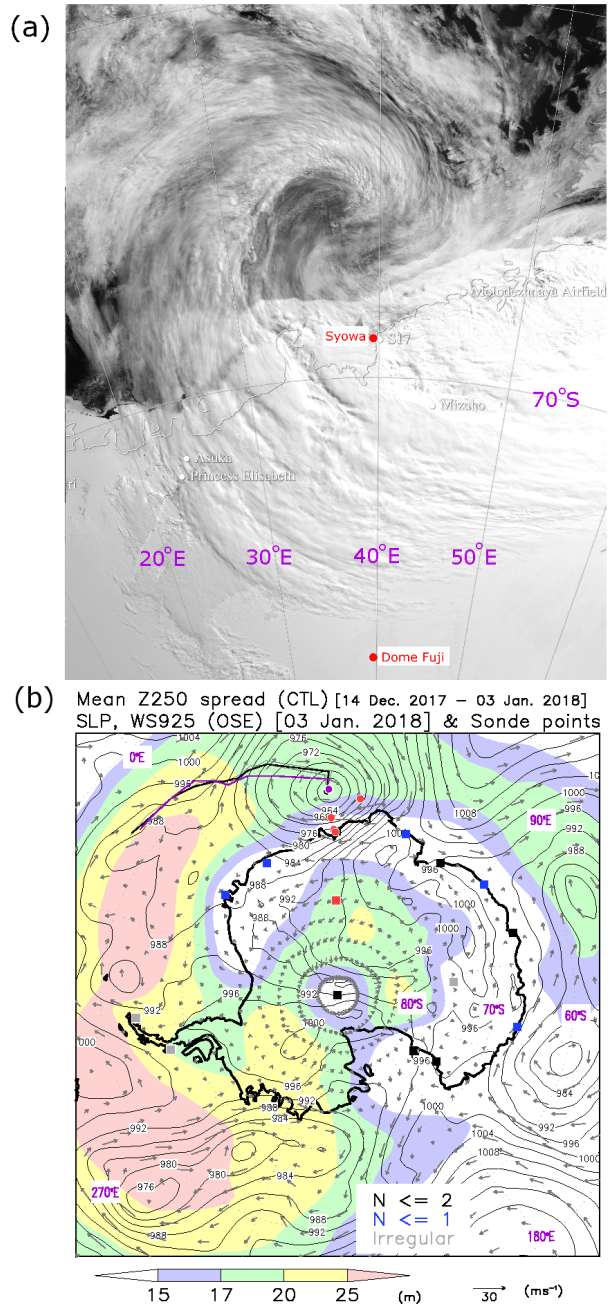

Fig. 1. (a) MODIS image acquired at 0605 UTC 3 January 2018. White dots indicate locations of research stations. (b) Monthly mean ensemble spread of geopotential height at 250 hPa in CTL (shading). Contours and vectors show SLP and wind fields (speed and direction) at 925 hPa at 0000 UTC 3 January 2018 in CTL. Squares and red dots show radiosonde launch points at Antarctic research stations and RV Shirase, respectively. Colors of squares indicate the frequency of daily radiosonde observations (N). The red square indicates the position of Dome Fuji Station. Purple and black lines show the cyclone track from 31 December 2017 to 3 January 2018 in OSE and ERA5, respectively.

(Reynolds et al., 2007).

In this study, two 63-member ensemble reanalysis datasets were constructed using ALEDAS2. ALERA2, which includes the observational data in the PREPBUFR global observation datasets, is the control reanalysis (CTL). Our additional radiosonde observations have not been included in NCEP's operational forecast system. The other reanalysis data comprise an OSE that has assimilated radiosonde observational data (temperature, mixing ratio and wind speed) from RV Shirase and Dome Fuji Station into CTL. To examine the predictability of extreme weather events, we also conducted two forecast experiments (hereafter referred to as CTLf and OSEf) initialized with CTL and OSE. ALERA2 (i.e., AFES), with a horizontal resolution of T239 (triangular truncation with truncation wavenumber 239) and 48 vertical levels, was used.

We calculated the ensemble spread as follows:

$$\sigma = \left[\sum_{i=1}^{n} \frac{(x_i - \bar{x})^2}{n} \right]^{\frac{1}{2}}, \tag{1}$$

$$\bar{x} = \sum_{i=1}^{n} \frac{x_i}{n}, \tag{2}$$

where x is a state value. The root-mean-square error (RMSE) was calculated as follows:

$$\mathrm{RMSE} = \left[\frac{1}{n} \sum_{i=1}^{n} [(\mathrm{SIM}x)_i - (\mathrm{OBS}x)_i]^2 \right]^{1/2},$$

where SIMx is a simulated value and OBSx is an observed value.

2.3. *Reanalysis and operational forecast data*

To investigate the performance of the reanalysis data, we used 6-h ERA5 reanalysis data with a horizontal resolution of 0.56°. ERA5, which is provided by the European Centre for Medium-Range Weather Forecasts (ECMWF), is a successor of ERA-Interim. In addition, medium-range ensemble forecast data from two operational numerical weather prediction centers—the ECMWF and Japan Meteorological Agency (JMA)—are available via the TIGGE data portal (Swinbank et al., 2016) and were used in this study. Model details are presented in Table 1. Incorporation of radiosonde observations from Dome Fuji Station represents the main difference between ECMWF and JMA forecasts. Neither operational weather center used the RV Shirase observations. The status of the Global Telecommunication System was monitored daily over the geographical coverage of

Table 1. Summary of operational medium-range ensemble forecast systems used in this study (see http://tigge.ecmwf.int/models.html for details).

Numerical weather prediction center	Forecast model resolution	Ensemble size	Output resolution
ECMWF	TL639L91	51	0.5° × 0.5°
JMA	TL479L60	27	0.5° × 0.5°

Table 2. Dome Fuji data assimilated in the ERA5 product.

Date (YYYY/MM/DD)	1200 UTC	1800 UTC	Lat (°S)	Lon (°E)
2017/12/21	○	○	77.8	39.1
2017/12/22	○	○	77.8	39.1
2017/12/23	○	○	77.8	39.1
2017/12/24	○	○	77.8	39.1
2017/12/25	○	×	77.8	39.1
2017/12/26	○	○	77.8	39.1
2017/12/27	○	○	77.8	39.1
2017/12/28	○	○	77.8	39.1
2017/12/29	○	○	77.8	39.1
2017/12/30	–	–	–	–
2017/12/31	○	○	77.6	41.0
2018/01/01	○	○	77.6	41.0
2018/01/02	○	○	77.6	41.0

Notes: ○ assimilated; × not assimilated, – no observation

the ECMWF (via https://www.ecmwf.int/en/forecasts/charts/monitoring/dcover) and monitoring results indicated that the additional radiosonde observations from Dome Fuji have been assimilated into the ECMWF forecasts. Dome Fuji observations that were assimilated into ERA5 are listed in Table 2. In contrast, JMA did not assimilate Dome Fuji data because it does not use observations from Mobile TEMP (JMA, personal communication).

3. Results

3.1. *Revised reanalysis data with radiosonde observation*

The monthly mean ensemble spread of geopotential height at 250 hPa (Z250; Fig 1b) based on the ensemble spread of the 63 members of CTL was computed to estimate the uncertainty in the analysis and reanalysis data. The ensemble spreads of Z250 were small at coastal sites and near the South Pole, indicating that regular radiosonde observations at these locations lowered the ensemble spread, even in CTL. In contrast, the ensemble spreads of Z250 were large over the Pacific and Atlantic sectors of the Southern Ocean, Weddell Sea, and continental parts of East Antarctica in CTL because of the lack of radiosonde observations. The large ensemble spread of Z250 would influence the skill in reproducing atmospheric circulation over the Southern Hemisphere. Figure 1b shows a relatively large ensemble spread of Z250 in the area around Dome Fuji Station; thus, incorporation of additional radiosonde data from this area would reduce the ensemble spread of Z250 in ana-

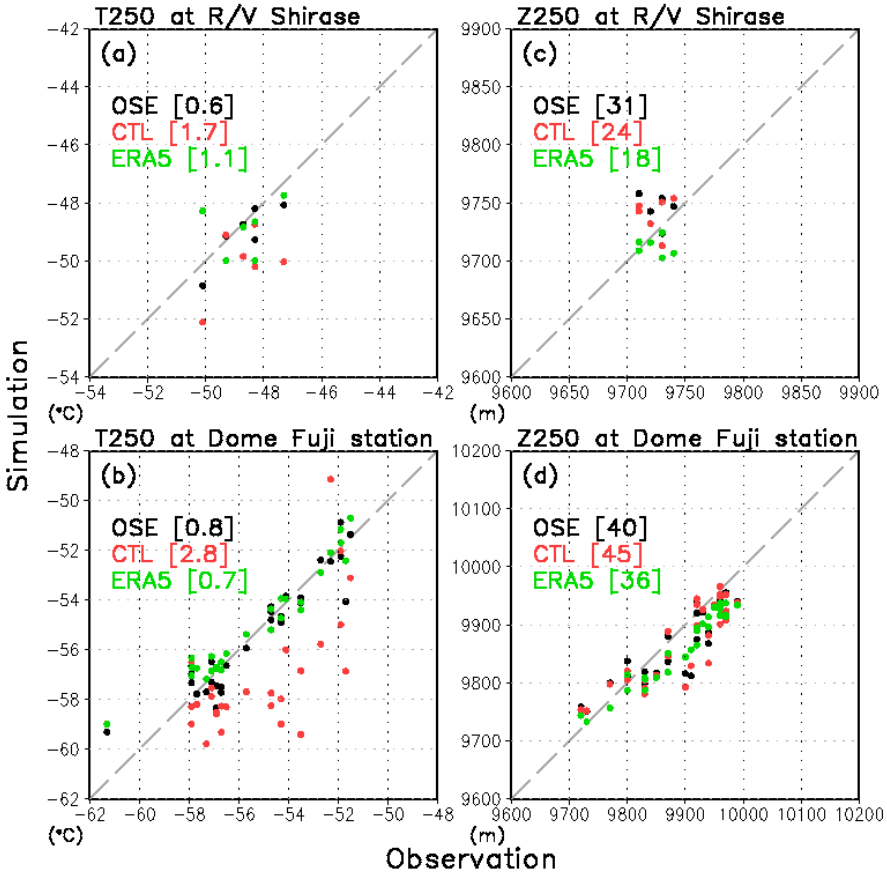

Fig. 2. Scatterplots of simulated temperature at 250 hPa (green, ERA5; black, OSE; red, CTL) and temperature measured by radiosondes at (a) RV Shirase and (b) Dome Fuji Station. Squares indicate the temperature measured at 1800 UTC for each day. (c, d) As in (a, b) but for geopotential height at 250 hPa. Values are the RMSE for each reanalysis dataset.

lysis and reanalysis data.

Scatterplots of observed and simulated (OSE, CTL, and ERA5) temperatures at 250 hPa are presented in Fig. 2 to allow comparison between observational data and the results of ensemble reanalysis products at the tropopause. The plots show data from the grid point nearest to observation points at the time of each radiosonde release. Although OSE captured the temperature measured by RV Shirase's radiosondes with temperature biases of less than 1°C at the site of RV *Shirase*, there were temperature biases at 250 hPa in CTL (Fig. 2a). Temperature biases in ERA5 occasionally exceeded 1°C, but their magnitudes remained small, indicating that assimilation of satellite data enhances ERA5's performance. The RMSE of temperature at 250 hPa in OSE (0.6) was smaller than that in CTL (1.7) and ERA5 (1.1). However, ERA5 and OSE adequately reproduced the temperature at 250 hPa at Dome Fuji Station because of the assimilation of additional radiosonde observations (Fig. 2b). In contrast, CTL included no additional radiosonde data and generally had large temperature biases. Therefore, the RMSE of CTL (2.8) was larger than that of OSE (0.8) and ERA5 (0.7).

For temperature in the upper troposphere at the approach of a cyclone, there are large overall differences between the results of OSEs and CTL experiments (Inoue et al., 2013; Sato et al., 2018b). Here, temperature differences were generally large at Dome Fuji Station (Fig. 2b), even in the absence of an approaching cyclonic system, indicating that the sparsity of radiosonde observations over Antarctica is causing large Z250 errors in analysis and reanalysis data over Dome Fuji. Temperature biases at the site of RV *Shirase* were smaller than those at Dome Fuji (Fig. 2a) because the daily/twice-daily radiosonde observations at Antarctic coastal operational stations (e.g., Syowa Station) would have already reduced errors at upper levels in the reanalysis data, even in the absence of additional ship-launched soundings. Therefore, in ERA5, the magnitude of mean temperature bias at the site of RV *Shirase* (1.0°C) was greater than that at Dome Fuji Station (−0.3°C). These results indicate that additional radiosonde observations at Dome Fuji Station have a substantial impact on temperature reproduction in reanalysis data.

3.2. *Improvement in forecasting cyclones over the Southern Ocean*

Bias in geopotential height in the tropopause would influence the prediction skill of a forecasting system. We assessed the impact of additional radiosonde observations on the reproduction of atmospheric circulation in forecast experiments by examining a cyclone near Antarctica. The cyclone was generated over the South Atlantic Ocean on 31 December 2017 and subsequently crossed the Southern Ocean (Fig. 1b). On 3 January 2018, it intensified near Syowa Station. Strong winds in the lower troposphere were observed near the coast and in the southeastern part of the cyclone (Fig. 3a). While the winds near the southeastern part of the cyclone had characteristics similar to those of barrier wind (O'Connor et al., 1988, 1994), strong winds associated with the cyclone were observed near Syowa Station, where winds exceeding 20 m s^{-1} were recorded on 3 January 2018 at the surface. In the OSE reanalysis, wind speeds at 925 hPa at 0000 UTC 3 January exceeded 24 m s^{-1} at the grid point nearest to Syowa Station. A trough at 500 hPa extended to the Southern Ocean, influencing the cyclone's development and position (contours in Fig. 3e). Integrated water vapor (IWV) from 925 to 300 hPa near the coast of Antarctica is represented by the shading in Fig. 3e. Intense snowfall associated with strong moisture transport influences not only human activity at Antarctic research stations, but also the surface mass balance of the Antarctic ice sheet (Hirasawa et al., 2013; Gorodetskaya et al., 2014).

The 63-member ensemble predictions of mean wind speed at 925 hPa and SLP for a 2.5-day forecast initialized with the OSE and CTL focusing on this event are shown in Figs. 3b and c. The initial time was set to 1200 UTC 31 December 2017. Some ensemble members placed the center of the cyclone to the west of the observed one; neither CTLf nor OSEf captured the cyclone's location near Antarctica. However, the magnitudes of wind speed and SLP near the coast were smaller in CTLf than in OSEf (Figs. 3b, c and 4a), resulting in a difference in wind speed between OSEf and CTLf (Fig. 3d). In addition, the amount of IWV associated with strong poleward winds near the coast was captured in OSEf (Fig. 3f); however, the simulated magnitude (i.e., in OSE) was smaller than that observed. In contrast, CTLf was unable to correctly capture the amount of IWV near the coast because of its failure to forecast the strong winds (Fig. 3g). Between OSEf and CTLf, the differences in the cyclone's development led to differences in IWV near the coast (Fig. 3h).

The temporal evolution of the central pressure of the cyclone at the surface level in OSE, OSEf and CTLf (Fig. 4a) was analyzed to assess the impact of the additional Antarctic radiosonde observations on the skill in forecasting the cyclone's central pressure. In OSE, the cyclone developed rapidly from 1200 UTC 2 January 2018 and the ensemble mean central pressure reached 956 hPa at 0000 UTC 3 January. However, the value was smaller than that in ERA5 (black line in Fig. 4b), partly because of the difference in model resolution. Most members in OSEf captured the decrease in central pressure from 1200 UTC 2 January, whereas all members in CTLf tended to underestimate the development of the central pressure at 0000 UTC 3 January (Fig. 4a).

3.3. *Flow-dependent error at upper levels*

Above the western part of the surface cyclone the ensemble spreads of Z250 in OSEf and CTLf were different, indicating that a reasonably large ensemble spread in the trough was the reason for the failure to forecast the cyclone's development in CTLf (green contours in Fig. 3h). To investigate the origin of the large ensemble spread at the tropopause, we computed the difference between the ensemble spread of Z250 in OSEf and that in CTLf (ΔZ250) and

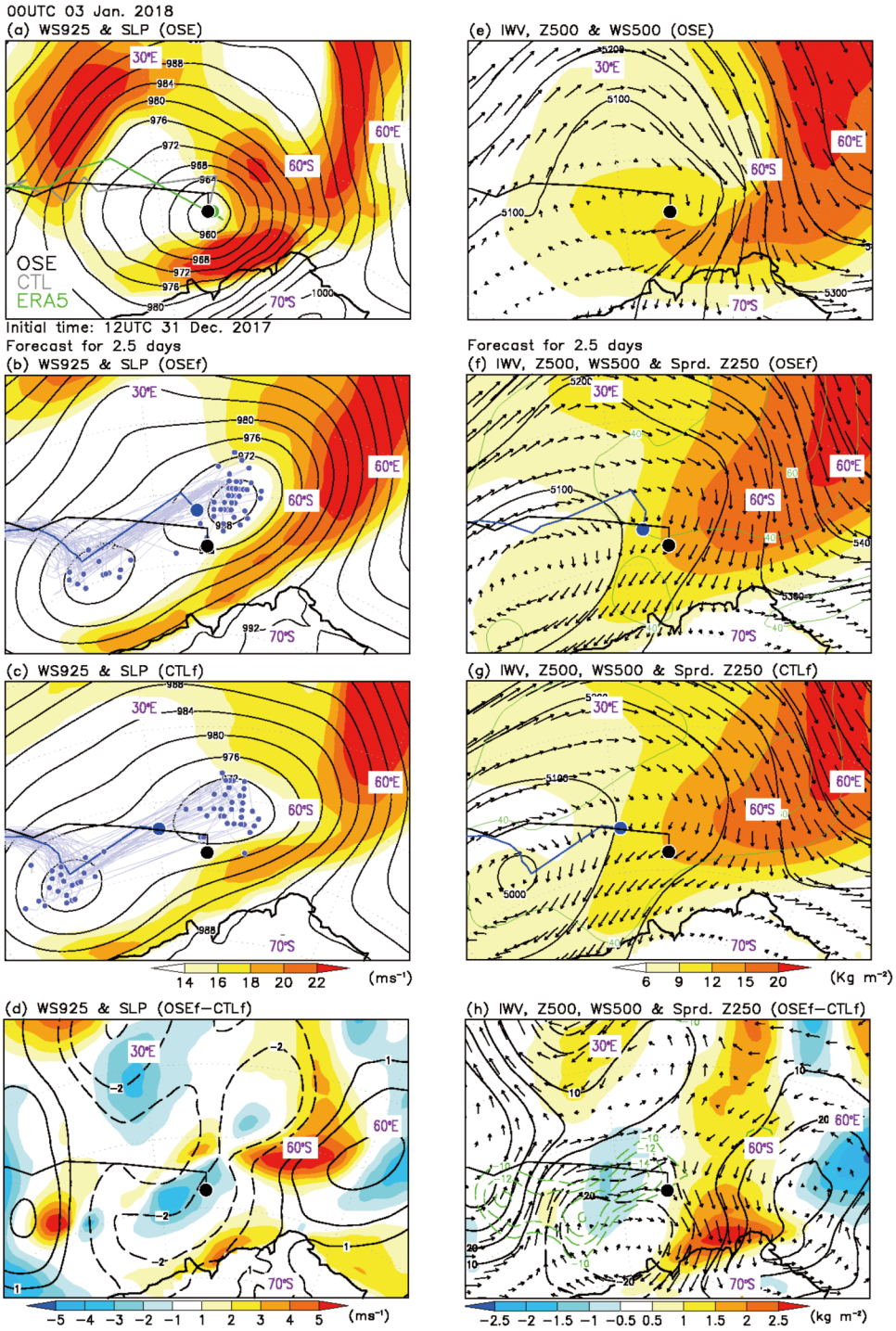

Fig. 3. Wind speed at the 925-hPa height (WS925) (shading; units: m s^{-1}) with SLP (contours; units: hPa) at 0000 UTC 3 January 2018 in (a) OSE, (b) OSEf, and (c) CTLf. (d) Differences in ensemble mean wind speed at WS925 (shading; units: m s^{-1}) and SLP (contours; units: hPa) between OSEf and CTLf. (a–d) Black, gray, and green lines indicate the cyclone track between 1200 UTC 31 December 2017 and 0000 UTC 3 January 2018 in OSE, CTL, and ERA5, respectively. (b) and (c) Blue lines indicate the predicted cyclone track between 1200 UTC 31 December 2017 and 0000 UTC 3 January 2018 in OSEf and CTLf, respectively. Thick lines indicate the ensemble mean. Thin lines indicate ensemble members. Blue dots indicate the predicted cyclone location at 0000 UTC 3 January 2018. Large dots indicate the ensemble mean. Small dots indicate ensemble members. (e–h) As in (a–d) but for the IWV from 925 to 300 hPa (shading; units: kg m^{-2}), geopotential height (contours; units: m), wind speed (vectors; units: m s^{-1}) at 500 hPa, and the ensemble spread of geopotential height at 250 hPa (green contours; units: m).

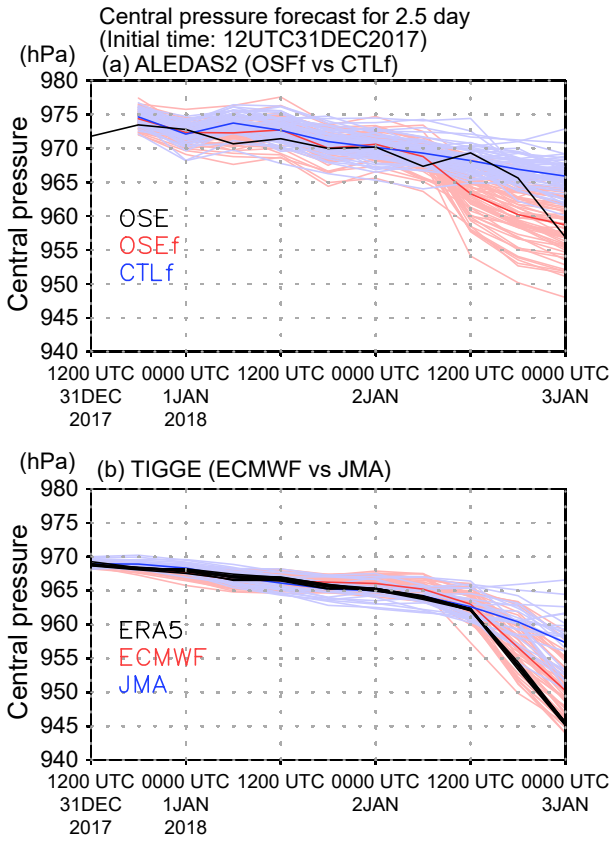

Fig. 4. Temporal evolution of cyclone central pressure in (a) OSE (black), OSEf (red) and CTLf (blue), and (b) ERA5, (black) ECMWF (red) and JMA (blue). Thick lines indicate the ensemble mean. Thin lines indicate ensemble members.

examined its temporal evolution. The ΔZ250 was used as a measure of the reduction in the ensemble spread as a result of the incorporation of additional radiosonde data. The maximum value point of ΔZ250 (MVPΔZ250) is a useful parameter for understanding the origin of ensemble spread at the tropopause (Sato et al., 2017, 2018a), and it was calculated and interpreted as action centers of the ΔZ250 fields for each time step. At the initial time, MVPΔZ250 was found near South Georgia and the South Sandwich Islands (54.50°S, 37.00°W; Fig. 5a). Over the forecast period, it moved along the trough over the Southern Ocean, and reached the western part of the cyclone at 0000 UTC 3 January 2018 (dots in Fig 5a). The MVPΔZ250 was near Dome Fuji Station on 27 December 2017, before then traveling with the strong background wind from the Antarctic Peninsula toward the Southern Ocean (squares in Fig 5a). Figure 5b shows the temporal evolution of MVPΔZ250. The difference in the ensemble spread of Z250 grew with an increase in lead time, even in the reanalysis data (before 1200 UTC 31 December 2017) because of the sparse observational network over Antarctica. It decreased by 9 m after 1200 UTC 30 December, when the large ensemble spread reached the Southern Ocean (Fig. 1). These results indicate that the incorporation of additional radiosonde observations over Antarctica reduces the ensemble spread at the tropopause in reanalysis data, which enhances the accuracy in the prediction of surface-level cyclonic development over the Southern Ocean.

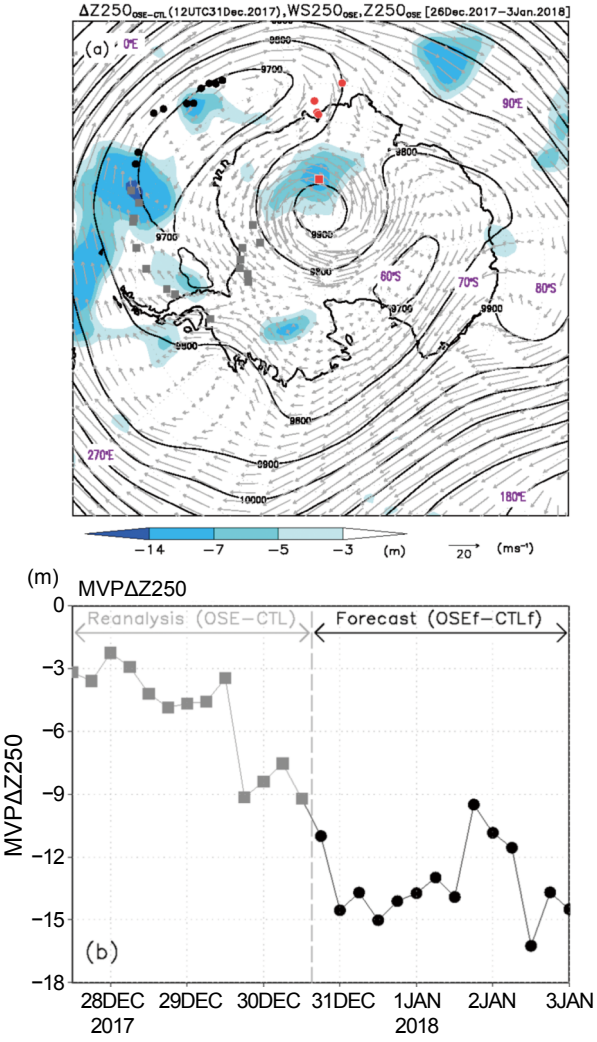

Fig. 5. (a) The difference (ΔZ250) between the mean ensemble spread of geopotential height at 250 hPa (Z250) in OSE and that in CTL at the initial time (shading; units: m), mean analysis Z250 (contours; units m), and wind speed (vectors; units: m s^{-1}) at 250 hPa (WS250) in OSE from 27 December 2017 to 3 January 2018. Gray squares (black dots) are maximum value points of the difference in Z250 (MVPΔZ250) between OSE and CTL (OSEf and CTLf). Red squares and dots show the locations of Dome Fuji and RV Shirase. (b) Temporal evolution of MVPΔZ250 between OSEf and CTLf before (squares) and during (dots) the forecast period.

4. Discussion

This study has revealed that the assimilation of radiosonde observations from RV Shirase and Dome Fuji Station improved the reproduction of atmospheric structures at the tropopause over the Antarctic continent, enhancing the skill in forecasting the surface-level circulation over the Southern Ocean. In this study, the impacts of satellite radi-

ance data on the reproduction of the Antarctic upper-level troposphere could not be assessed in our data assimilation system. However, from the point of view of observing system design, a flow-dependent error propagation associated with a trough is an essential concept that is universally applicable.

Forecasts from different operational forecast centers assimilated different quantities of additional radiosonde observations from Dome Fuji Station; thus, the skill in forecasting the cyclone case should vary between centers. To verify this, we compared the skill of ECMWF to that of JMA in predicting the cyclone case. ECMWF has assimilated Dome Fuji radiosonde observations (Table 2). The cyclone's development was predicted accurately in most members of ECMWF, as was the case in ERA5 (Fig. 4b). In contrast, JMA did not assimilate Dome Fuji radiosonde observations, and most members of JMA were unable to accurately reproduce the cyclone's central pressure. Although SLP in OSE was larger than that in ERA5 because of the difference in the quantity of assimilated satellite data, these characteristics were also reproduced in a comparison between OSEf and CTLf (Fig. 4a), suggesting that the incorporation of additional radiosonde observations from Dome Fuji Station would be very effective in the operational forecasting of cyclone central pressure over the Southern Ocean.

Because of the sparsity of observations over Antarctica compared with the Arctic, the period of accurate prediction with respect to atmospheric circulation in the Southern Hemisphere is shorter than that in the Northern Hemisphere (Jung and Matsueda, 2016). Therefore, even with the assimilation of additional Antarctic observations, OSE was unable to capture the cyclone's development in a 4.0-day forecast, suggesting that additional twice-daily radiosonde observations would be insufficient to improve the accuracy of cyclone prediction with a long lead time. Therefore, to investigate the impact of radiosonde observations on the skill to forecast cyclones in the Southern Hemisphere, greater numbers of additional observations are necessary. An enhanced observational network was established in the Antarctic from mid-November 2018 to mid-February 2019 under the program of the Year of Polar Prediction. During this period, many stations (including Syowa) undertook additional radiosonde observations at 0600 (and hopefully 1800) UTC, in conjunction with routine operational observations (0000 and 1200 UTC), thus providing an opportunity to investigate the role of additional Antarctic radiosonde observations in the reproduction of observed atmospheric circulation over the midlatitudes of the Southern Hemisphere.

Acknowledgments. This work was supported by a Japan Society for the Promotion of Science (JSPS) Overseas Research Fellowship, JSPS Grants-in-Aid for Scientific Research (KAKENHI) (Grant Nos. 19K14802 and 18H05053). We would like to thank the anonymous reviewers, whose constructive comments improved the quality of this manuscript. The authors thank the crew of RV "Shirase". The MODIS dataset received at Syowa Station is archived and provided by the Arctic Data archive System (ADS) developed by the National Institute of Polar Research. The ADS transferred radiosonde data from RV "Shirase" and Dome Fuji Station to the JMA. The TIGGE and ERA5 datasets are available via the ECMWF data portal (http://apps.ecmwf.int/datasets/). The ALEDAS2 and AFES integrations were performed on the Earth Simulator with the support of JAMSTEC. PREPBUFR, compiled by the NCEP and archived at the University Corporation for Atmospheric Research, was used as the observations (available from http://rda.ucar.edu). The datasets provided by ALEDAS2 were from JAMSTEC's website (http://www.jamstec.go.jp/alera/alera2.html). We thank James BUXTON MSc and Tin TIN PhD from Edanz Group (www.edanzediting.com./ac) for correcting drafts of this manuscript.

REFERENCES

Bracegirdle, T. J., 2013: Climatology and recent increase of westerly winds over the Amundsen Sea derived from six reanalyses. *International Journal of Climatology*, **33**, 843–851, https://doi.org/10.1002/joc.3473.

Bracegirdle, T. J., and G. J. Marshall, 2012: The reliability of Antarctic tropospheric pressure and temperature in the latest global reanalyses. *J. Climate*, **25**(20), 7138–7146, https://doi.org/10.1175/JCLI-D-11-00685.1.

Bromwich, D. H., J. P. Nicolas, and A. J. Monaghan, 2011: An Assessment of Precipitation Changes over Antarctica and the Southern Ocean since 1989 in Contemporary Global Reanalyses.*J.Climate*,**24**,4189–4209,https://doi.org/10.1175/2011JCLI4074.1.

Dee, D. P., and Coauthors, 2011: The ERA-interim reanalysis: Configuration and performance of the data assimilation system. *Quart. J. Roy. Meteor. Soc.*, **137**, 553–597, https://doi.org/10.1002/qj.828.

Enomoto, T., A. Kuwano-Yoshida, N. Komori, and W. Ohfuchi, 2008: Description of AFES 2: Improvements for high-resolution and coupled simulations. High Resolution Numerical Modelling of the Atmosphere and Ocean, K. Hamilton and W. Ohfuchi, Eds., Springer, 77–97, https://doi.org/10.1007/978-0-387-49791-4_5.

Enomoto, T., T. Miyoshi, Q. Moteki, Q., J. Inoue, M. Hattori, S. Kuwano-Yoshida, N. Komori, and S. Yamane, 2013: Observing-system research and ensemble data assimilation at JAMSTEC. Data Assimilation for Atmospheric, Oceanic and Hydrologic Applications (Vol. II), S. K. Park and L. Xu, Eds., Springer, 509–526, https://doi.org/10.1007/978-3-642-35088-7_21.

Gelaro, R., and Coauthors, 2017: The modern-era retrospective analysis for research and applications, version 2 (MERRA-2). *J. Climate*, **30**, 5419–5454, https://doi.org/10.1175/JCLI-D-16-0758.1.

Gorodetskaya, I. V., M. Tsukernik, K. Claes, M. F. Ralph, W. D. Neff, and N. P. M. Van Lipzig, 2014: The role of atmo-

spheric rivers in anomalous snow accumulation in East Antarctica. *Geophys. Res. Lett.*, **41**, 6199–6206, https://doi.org/10.1002/2014GL060881.

Hirasawa, N., H. Nakamura, H. Motoyama, M. Hayashi, and T. Yamanouchi, 2013: The role of synoptic-scale features and advection in prolonged warming and generation of different forms of precipitation at Dome Fuji station, Antarctica, following a prominent blocking event. *J. Geophys. Res. Atmos.*, **118**(13), 6916–6928, https://doi.org/10.1002/jgrd.50532.

Hunt, B. R., E. J. Kostelich, and I. Szunyogh, 2007: Efficient data assimilation for spatiotemporal chaos: A local ensemble transform Kalman filter. *Physica D: Nonlinear Phenomena*, **230**, 112–126, https://doi.org/10.1016/j.physd.2006.11.008.

Inoue, J., T. Enomoto, T. Miyoshi, and S. Yamane, 2009: Impact of observations from Arctic drifting buoys on the reanalysis of surface fields. *Geophys. Res. Lett.*, **36**, L08501, https://doi.org/10.1029/2009GL037380.

Inoue, J., M. E. Hori, T. Enomoto, and T. Kikuchi, 2011: Intercomparison of surface heat transfer near the Arctic marginal ice zone for multiple reanalyses: A case study of September 2009. *SOLA*, **7**, 57–60, https://doi.org/10.2151/sola.2011-015.

Inoue, J., T. Enomoto, and M. E. Hori, 2013: The impact of radiosonde data over the ice-free Arctic Ocean on the atmospheric circulation in the Northern Hemisphere. *Geophys. Res. Lett.*, **40**, 864–869, https://doi.org/10.1002/grl.5020-7.

Inoue, J., A. Yamazaki, J. Ono, K. Dethloff, M. Maturilli, R. Neuber, R. Edwards, and H. Yamaguchi, 2015: Additional Arctic observations improve weather and sea-ice forecasts for the Northern Sea Route. *Scientific Reports*, **5**, 16868, https://doi.org/10.1038/srep16868.

Jakobson, E., T. Vihma, T. Palo, L. Jakobson, H. Keernik, and J. Jaagus, 2012: Validation of atmospheric reanalyses over the central Arctic Ocean. *Geophys. Res. Lett.*, **39**, L10802, https://doi.org/10.1029/2012GL051591.

Jones, P. D., and D. H. Lister, 2015: Antarctic near-surface air temperatures compared with ERA-Interim values since 1979. *International Journal of Climatology*, **35**(7), 1354–1366, https://doi.org/10.1002/joc.4061.

Jones, R. W., I. A. Renfrew, A. Orr, B. G. M. Webber, D. M. Holland, and M. A. Lazzara, 2016: Evaluation of four global reanalysis products using in situ observations in the Amundsen Sea Embayment, Antarctica. *J. Geophys. Res. Atmos.*, **121**, 6240–6257, https://doi.org/10.1002/2015JD024680.

Jung, T., and M. Matsueda, 2016: Verification of global numerical weather forecasting systems in polar regions using TIGGE data. *Quart. J. Roy. Meteor. Soc.*, **142**, 574–582, https://doi.org/10.1002/qj.2437.

Jung, T., and Coauthors, 2016: Advancing polar prediction capabilities on daily to seasonal time scales. *Bull. Amer. Meteor. Soc.*, **97**, 1631–1647, https://doi.org/10.1175/BAMS-D-14-00246.1.

Kobayashi, S., and Coauthors, 2015: The JRA-55 reanalysis: General specifications and basic characteristics. *J. Meteor. Soc. Japan. Ser. II*, **93**(1), 5–48, https://doi.org/10.2151/jmsj.2015-001.

Kristjánsson, J. E., and Coauthors, 2011: The Norwegian IPY-THORPEX: Polar lows and Arctic fronts during the 2008 Andøya Campaign. *Bull. Amer. Meteor. Soc.*, **92**, 1443–1466, https://doi.org/10.1175/2011BAMS2901.1.

Miyoshi, T., and S. Yamane, 2007: Local ensemble transform Kalman filtering with an AGCM at a T159/L48 resolution. *Mon. Wea. Rev.*, **135**, 3841–3861, https://doi.org/10.1175/2007MWR1873.1.

O'Connor, W. P., and D. H. Bromwich, 1988: Surface airflow around Windless Bight, Ross Island, Antarctica. *Quart. J. Roy. Meteor. Soc.*, **114**, 917–938, https://doi.org/10.1002/qj.49711448205.

O'Connor, W. P., D. H. Bromwich, and J. F. Carrasco, 1994: Cyclonically forced barrier winds along the Transantarctic Mountains near Ross Island. *Mon. Wea. Rev.*, **122**(1), 137–150, https://doi.org/10.1175/1520-0493(1994)122<0137:CFBWAT>2.0.CO;2.

Ohfuchi, W., and Coauthors, 2004: 10-km mesh meso-scale resolving simulations of the global atmosphere on the Earth Simulator-Preliminary outcomes of AFES (AGCM for the Earth Simulator). *Journal of the Earth Simulator*, **1**, 8–34.

Powers, J. G., 2007: Numerical prediction of an Antarctic severe wind event with the weather research and forecasting (WRF) model.*Mon.Wea.Rev.*,**135**,3134–3157,https://doi.org/10.1175/MWR3459.1.

Reynolds, R. W., T. M. Smith, C. Y. Liu, D. B. Chelton, K. S. Casey, and M. G. Schlax, 2007: Daily high-resolution-blended analyses for sea surface temperature. *J. Climate*, **20**, 5473–5496, https://doi.org/10.1175/2007JCLI1824.1.

Rinke, A., Y. F. Ma, L. G. Bian, Y. F. Xin, K. Dethloff, P. O. G. Persson, C. Lu?pkes, and C. D. Xiao, 2012: Evaluation of atmospheric boundary layer-surface process relationships in a regional climate model along an East Antarctic traverse. *J. Geophys. Res. Atmos.*, **117**, D09121, https://doi.org/10.1029/2011JD016441.

Rinke, A., K. Dethloff, W. Dorn, D. Handorf, and J. C. Moore, 2013: Simulated Arctic atmospheric feedbacks associated with late summer sea ice anomalies. *J. Geophys. Res. Atmos.*, **118**, 7698–7714, https://doi.org/10.1002/jgrd.50584.

Saha, S., and Coauthors, 2010: The NCEP climate forecast system reanalysis. *Bull. Amer. Meteor. Soc.*, **91**(8), 1015–1058, https://doi.org/10.1175/2010BAMS3001.1.

Saha, S., and Coauthors, 2014: The NCEP climate forecast system version 2. *J. Climate*, **27**, 2185–2208, https://doi.org/10.1175/JCLI-D-12-00823.1.

Sato, K., J. Inoue, A. Yamazaki, J.-H. Kim, M. Maturilli, K. Dethloff, S. R. Hudson, and M. A. Granskog, 2017: Improved forecasts of winter weather extremes over midlatitudes with extra Arctic observations. *J. Geophys. Res. Oceans*, **122**, 775–787, https://doi.org/10.1002/2016JC012197.

Sato, K., J. Inoue, A. Yamazaki, J.-H. Kim, A. Makshtas, V. Kustov, M. Maturilli, and K. Dethloff, 2018a: Impact on predictability of tropical and mid-latitude cyclones by extra Arctic observations. *Scientific Reports*, **8**, 12104, https://doi.org/10.1038/s41598-018-30594-4.

Sato, K., J. Inoue, S. P. Alexander, G. McFarquhar, and A. Yamazaki, 2018b: Improved reanalysis and prediction of atmospheric fields over the Southern Ocean using campaign-based radiosonde observations. *Geophys. Res. Lett.*, **45**, 11, https://doi.org/10.1029/2018GL079037.

Semmler, T., M. A. Kasper, T. Jung, and S. Serrar, 2016: Remote impact of the Antarctic atmosphere on the Southern mid-latitudes. *Meteor. Z.*, **25**, 71–77, https://doi.org/10.1127/metz/2015/0685.

Soldatenko, S., C. Tingwell, P. Steinle, and B. A. Kelly-Gerreyn, 2018: Assessing the impact of surface and upper-air observations on the forecast skill of the ACCESS numerical weather prediction model over Australia. *Atmosphere*, **9**(1), 23,

https://doi.org/10.3390/atmos9010023.

Swinbank, R., and Coauthors, 2016: The TIGGE project and its achievements. *Bull. Amer. Meteor. Soc.*, **97**(1), 49–67, https://doi.org/10.1175/BAMS-D-13-00191.1.

Yamazaki, A., J. Inoue, K. Dethloff, M. Maturilli, and G. König-Langlo, 2015: Impact of radiosonde observations on forecasting summertime Arctic cyclone formation. *J. Geophys. Res. Atmos.*, **120**, 3249–3273, https://doi.org/10.1002/2014JD022925.

Yamagami, A., M. Matsueda, and H. L. Tanaka, 2017: Extreme arctic cyclone in August 2016. *Atmospheric Science Letters*, **18**, 307–314, https://doi.org/10.1002/asl.757.